Response of water isotopes in precipitation to a collapse of the West Antarctic Ice Sheet in high-resolution simulations with the Weather Research and Forecasting Model

Marina Dütsch[a,b] , Eric J. Steig[b,c] , Peter N. Blossey[c] , Andrew G. Pauling[c]

[a] *Department of Meteorology and Geophysics, University of Vienna, Vienna, Austria*

[b] *Department of Earth and Space Sciences, University of Washington, Seattle, WA, USA*

[c] *Department of Atmospheric Sciences, University of Washington, Seattle, WA, USA*

Corresponding author: Marina Dütsch, marina.duetsch@univie.ac.at

Early Online Release: This preliminary version has been accepted for publication in *Journal of Climate*, may be fully cited, and has been assigned DOI 10.1175/JCLI-D-22-0647.1. The final typeset copyedited article will replace the EOR at the above DOI when it is published.

ABSTRACT: The West Antarctic Ice Sheet (WAIS) may have collapsed during the last interglacial period, between 132,000 and 116,000 years ago. The changes in topography resulting from WAIS collapse would be accompanied by significant changes in Antarctic surface climate, atmospheric circulation, and ocean conditions. Evidence of these changes may be recorded in water-isotope ratios in precipitation archived in the ice. We conduct high-resolution simulations with an isotope-enabled version of the Weather Research and Forecasting Model over Antarctica, with boundary conditions provided by climate-model simulations with both present-day and lowered WAIS topography. The results show that while there is significant spatial variability, WAIS collapse would cause detectable isotopic changes at several locations where ice-core records have been obtained or could be obtained in the future. The most robust signals include elevated δ^{18}O at SkyTrain Ice Rise in West Antarctica, and elevated deuterium excess at Hercules Dome in East Antarctica. A combination of records from multiple sites would provide constraints on the timing, rate, and magnitude of past WAIS collapse.

Accepted for publication in *Journal of Climate*. DOI 10.1175/JCLI-D-22-0647.1.

1. Introduction

The West Antarctic Ice Sheet (WAIS) has the potential to contribute as much as 3.3 m to global eustatic sea level (Bamber et al. 2009). Since much of the bedrock beneath the WAIS lies below sea level, the removal of fringing ice shelves would lead to a rapid inland migration of the grounding line and large-scale deglaciation ("collapse") of the WAIS (Mercer 1978; Pollard and DeConto 2009). Evidence that the WAIS has collapsed in the past, coupled with knowledge of the climate conditions that led to collapse, is important for evaluating the likelihood of future collapse.

The possibility of WAIS collapse during the last interglacial period, the Eemian (132 to 116 thousand years ago (ka)), is of particular interest because the global average temperature was less than 1.5°C warmer than today (Turney and Jones 2010; McKay et al. 2011; Fischer et al. 2018). WAIS collapse during the Eemian is likely, given that eustatic sea level was as much as 4 – 9 m higher (Kopp et al. 2009; Dutton and Lambeck 2012; Dyer et al. 2021), but direct evidence is lacking. The only unambiguous evidence of WAIS collapse during the Pleistocene (2,580 to 12 ka) comes from sediment cores: Scherer et al. (1998) found Quaternary diatoms and high concentrations of meteoric ^{10}Be in sediment samples beneath a West Antarctic ice stream, requiring that open marine conditions existed in the southern part of the Ross Sea sector of the ice sheet (see Supplementary Figure S1 for a map showing all locations mentioned in the text). Similarly, it should be possible to use cosmogenic-isotope exposure dating in bedrock samples obtained from beneath the present-day ice sheet to obtain additional evidence for or against Eemian collapse (Spector et al. 2018). However, cosmogenic isotope ratios generally reflect the integrated history of burial and exposure, rather than discrete events (see, e.g., the results of Schaefer et al. (2016) for the Greenland Ice Sheet), which may limit their precision for constraining the rate and timing of WAIS collapse.

An alternative approach to determining whether – and if so, how quickly – the WAIS collapsed during the Eemian is the analysis of ice cores, which can be accurately dated through a combination of annual-layer counting, identification of stratigraphic horizons, and cross dating with other records (WAIS Divide Project Members 2013; Bazin et al. 2013; Veres et al. 2013). The large changes in Antarctic ice sheet topography associated with a collapse of the WAIS would likely impact temperature and atmospheric circulation over the ice sheet, as well as the water-isotope ratios that are archived in the ice. Most existing ice-core records that extend through the Eemian

Accepted for publication in *Journal of Climate*. DOI 10.1175/JCLI-D-22-0647.1.

are from locations on the East Antarctic plateau (e.g., Masson-Delmotte et al. 2011), but the largest changes in water-isotope ratios resulting from a collapse of the WAIS are expected in West Antarctica and nearby regions. A horizontal ice trench from the Mount Moulton Blue Ice Area (Popp 2008; Korotkikh et al. 2011; Steig et al. 2015) is the only published West Antarctic record containing Eemian ice, but a new core obtained at SkyTrain Ice Rise (Mulvaney et al. 2021) in 2019 may contain Eemian ice as well. A future ice core from Hercules Dome, planned for 2025, is of particular interest; while Hercules Dome is in East Antarctica, it lies at the edge of the Transantarctic Mountains adjacent to West Antarctica, and the climate impact there may be relatively large for an East Antarctic site. Colder conditions at Hercules Dome than at SkyTrain Ice Rise increase the likelihood of obtaining a complete Eemian record (Jacobel et al. 2005; Fudge et al. 2022).

Previous climate-model results suggest that in combination, records from SkyTrain Ice Rice, Mount Moulton, and Hercules Dome, could provide valuable constraints on the history of the WAIS. For example, Steig et al. (2015) used several climate models, including the isotope-enabled European Center Hamburg Model version 4.6 (Hoffmann et al. 1998) and found that a lower WAIS should be associated with lower temperatures and reduced δ^{18}O at Mount Moulton, and higher temperature and δ^{18}O at Hercules Dome, relative to sites in interior East Antarctica. Similarly, Holloway et al. (2016) and Goursaud et al. (2021), using the isotope-enabled Hadley Centre Climate model (Tindall et al. 2009), found elevated temperatures and δ^{18}O across most of West Antarctica and adjacent regions in East Antarctica. However, all of these studies used general circulation models with relatively coarse horizontal resolutions, which do not resolve small-scale topographic features that may have a significant influence on the local climate and isotopes in precipitation at the specific locations where ice cores are obtained. Furthermore, while Steig et al. (2015) used realistic topography from the ice-sheet-model simulations of Pollard and DeConto (2009), both Holloway et al. (2016) and Goursaud et al. (2021), as well as most earlier work (e.g., Holden et al. 2010; Otto-Bliesner et al. 2013) used simpler, idealized topography. Justino et al. (2015) used realistic ice-sheet topography but much lower climate-model resolution (3.75°). No study to date has analyzed the impact of WAIS collapse on the second-order isotope parameter deuterium excess ("d-excess"), defined as $\delta\mathrm{D} - 8 \cdot \delta^{18}\mathrm{O}$, which responds to different processes and might reveal valuable complementary information to δ^{18}O.

Accepted for publication in *Journal of Climate*. DOI 10.1175/JCLI-D-22-0647.1.

In this study, we use the Weather Research and Forecasting Model (WRF, Skamarock and Klemp 2008) version 3.9.1, modified to include water isotopes, to perform high-resolution simulations of Antarctic climate in scenarios where the WAIS has collapsed, and compare them with control simulations, in which the WAIS is intact. Our particular goal is to evaluate how a WAIS collapse could be detected in δ^{18}O and d-excess records in or near West Antarctica that do, or are likely to, contain Eemian ice.

2. Methods

We conducted simulations with a new water-isotope-enabled implementation of the Weather Research and Forecasting model (WRF, Skamarock and Klemp 2008), which we call WRFwiso. Moore et al. (2016) made an initial implementation of water isotopes in the WRF model to study the isotopic composition of orographic precipitation, which included the advection and diffusion of stable water isotopes as well as their integration into the Thompson et al. (2008) microphysical scheme. We extended that implementation to enable grid nesting and to allow water isotope information to be drawn from externally-derived initial and boundary conditions. We also integrated water isotopes into the Mellor-Yamada-Janjic planetary boundary layer (PBL) scheme (Janjić 2001) and the Eta similarity surface layer scheme (Janjic 1996). We did not implement water isotope parameterizations in the convection schemes in this version of WRFwiso, since convection is relatively unimportant at high latitudes. These could be implemented in the future for mid latitude and tropical applications when coarse horizontal resolutions are used. In the following, the implementation of water isotopes is described in more detail.

Throughout the manuscript, water isotope values are reported in per mil (‰) using the conventional notation, i.e., $\delta^{18}\mathrm{O} = {}^{18}R/R_{VSMOW}\text{-}1$, $\delta\mathrm{D} = {}^{2}R/R_{VSMOW}\text{-}1$, where ${}^{18}R$ is the relative abundance of ^{18}O to ^{16}O, ${}^{2}R$ is the relative abundance of D to H, and R_{VSMOW} refers to the composition of the Vienna Standard Mean Ocean Water standard.

a. Implementation of water isotopes in WRF

1) Surface fluxes

Except for upward moisture fluxes over land and sea ice, isotopic moisture fluxes from the surface are computed using the same bulk formulas used for $\mathrm{H_2^{16}O}$, except that the surface transfer coefficient

Accepted for publication in *Journal of Climate*. DOI 10.1175/JCLI-D-22-0647.1.

is scaled by the kinetic fractionation factor $(1+k)$, where k is computed following equation 11 in Merlivat and Jouzel (1979), and the surface moisture is computed as $R_{sfc}q_{sfc}/\alpha_{eq}(T_{sfc})$. Here, T_{sfc}, q_{sfc} and R_{sfc} are the surface temperature, the available moisture for evaporation at the surface (i.e., the saturation specific humidity over the ocean) and the isotopic ratio of the surface waters, respectively, while α_{eq} is the equilibrium fractionation coefficient computed as in Majoube (1971) for liquid and Majoube (1970) and Merlivat and Nief (1967) for ice. Because water isotopes are not integrated into the land surface and sea ice parameterizations, the isotopic content of surface waters (i.e., soil moisture or snow/ice surfaces) are prescribed by inputs to the model, which may vary in space and time. The isotopic composition of ocean water is assumed to be that of Vienna Standard Mean Ocean Water for the WRFwiso simulations in this paper, though it may also be prescribed to vary in space and time. The isotopic composition of upward fluxes from the land surface (including the ice sheet surface) and sea ice are assumed to be non-fractionating, so that their isotopic composition is fixed to the prescribed value of R_{sfc}. This assumption models the upward fluxes over land and sea ice as corresponding approximately to transpiration or non-fractionating sublimation of ice. The latter may be appropriate over Antarctica, though recent research suggests that sublimation from snow surfaces does fractionate (Wahl et al. 2021).

2) Microphysics

In the microphysical parameterization (Thompson et al. 2008), each transformation of water ($H_2^{16}O$), between vapor and hydrometeors and among the hydrometeors was duplicated for the heavy water isotopes, $H_2^{18}O$ and $HD^{16}O$. The transfer of water isotopes among water vapor and hydrometeors (cloud liquid, cloud ice, rain, snow and graupel) are modeled following appendix B of Blossey et al. (2010) and are summarized here briefly. Exchanges among liquid and ice phase hydrometeors (e.g., due to freezing or melting) are assumed to be non-fractionating, i.e., that the exchange of heavy isotope mass occurs in proportion to its mass ratio within the source hydrometeor, so that a raindrop resulting from a melting snowflake would have the same isotopic composition as the snow from which it was formed. Water vapor and cloud liquid are assumed to be in isotopic equilibrium, while isotopic fractionation (both equilibrium and kinetic) occurs during exchanges between rain and vapor, and also during water vapor deposition onto ice phase hydrometeors. Sublimation of ice phase hydrometeors, however, is assumed to be non-fractionating.

Accepted for publication in *Journal of Climate*. DOI 10.1175/JCLI-D-22-0647.1.

b. Simulation set-up

1) Model configuration

For the WRFwiso simulations, we used the Advanced Research WRF (ARW, version 3.9.1), configured with the Unified NOAH land surface model, the Monin-Obukhov (Janjic) surface layer scheme (Janjić 2001), the Mellor-Yamada-Janjic PBL scheme (Janjić 2001), the RRTMG radiation scheme for shortwave and longwave (Mlawer et al. 1997; Iacono et al. 2008), and the Thompson et al. (2008) microphysics scheme. We also adopted the modifications to some WRF routines contained in Polar WRF (Bromwich et al. 2013, version 3.9.1), which are optimized for simulations in polar regions.

WRFwiso was run for 9 years in two domains with one-way nesting. The outer domain has a horizontal resolution of 45 km and covers Antarctica and most of the Southern Ocean. The inner domain has a horizontal resolution of 15 km and covers Antarctica and small parts of the Southern Ocean. Both domains have 60 hybrid vertical levels (Park et al. 2019). WRFwiso was run separately for each month of the nine-year time period and initialized two days before the start of the month to allow time for spin-up. Those two spin-up days are discarded in the analysis here.

Initial and boundary conditions, including sea surface temperature, sea ice fraction, and the isotopic composition of fluxes over the ice and land surfaces, were provided by monthly climatologies from simulations with the isotope-enabled version of the Community Atmosphere Model (iCAM) (Nusbaumer et al. 2017; Brady et al. 2019; Dütsch et al. 2019), coupled to the isotope-enabled Community Land Model (iCLM) (Wong et al. 2017). We ran iCAM for 30 years at $0.9°\times1.25°$ resolution with 30 vertical levels, using pre-industrial ocean surface conditions from Hurrell et al. (2008). The last 28 years of the simulations were used for the analysis. A smaller set of years (4–20) was used to construct monthly climatologies of surface fields for forcing the WRFwiso simulations. Six-hourly outputs from simulation years 4–12 of iCAM provided initial conditions for WRFwiso and boundary conditions for the outer WRFwiso domain. Both WRFwiso domains apply spectral nudging to winds, temperature and geopotential heights above the PBL to keep the meteorology of WRFwiso close to that of iCAM on coarse spatial scales (~1000 km).

In all simulations, pre-industrial forcing (CO_2, orbital configuration, etc.) is used, and held fixed. We emphasize that these simulations are not intended to provide an estimate of last interglacial (Eemian) climate. Rather, they are idealized experiments intended to isolate the impact of topog-

Accepted for publication in *Journal of Climate*. DOI 10.1175/JCLI-D-22-0647.1.

raphy on the climate conditions that can potentially be recovered from measurements made on ice cores.

2) Topographic set-ups

Our simulations used two different topographic set-ups, similar to those in Steig et al. (2015): one in which modern topography is used everywhere, and another which includes significant lowering of the topography (i.e., "collapse") of the WAIS. The latter is taken from the ice-sheet model simulations of Pollard and DeConto (2009) at 700 ka before present, corresponding to the time (in that simulation) when the WAIS reaches its smallest size.

Figure 1 illustrates the WRFwiso model set-up, showing the 15 km and 45 km domains nested within the iCAM domain at 0.9°×1.25° resolution. *Control* refers to the simulation using modern topography, while *collapse* refers to the simulation using the lowered ice sheet topography. Both use the same pre-industrial ocean surface conditions and the same pre-industrial land-sea mask, in which the ice shelves are treated as "land" (i.e., covered by snow, and without sub-shelf ocean).

The pattern of WAIS collapse is to a great extent determined by the subglacial topography, but it also depends on the ice-sheet model and given climate boundary conditions. To evaluate the sensitivity of our results to different realizations of WAIS collapse we ran one additional iCAM simulation (*collapse G21*), for which we used the ice-sheet model output from Golledge et al. (2021) to compute the difference between WAIS collapse and modern topography. The difference in topography between *collapse G21* and *collapse* is shown in Supplementary Figure S2.

3) Ocean surface conditions

Changes to the Antarctic topography cause large-scale climate changes, including changes in sea surface temperature and sea ice that may in turn affect surface climate conditions, including isotope concentrations in precipitation (Steig et al. 2015). To assess the potential importance of this effect, we conducted additional iCAM experiments with ocean surface boundary conditions provided by results from fully-coupled climate model simulations with the Community Climate System Model version 4 (CCSM4) (Gent et al. 2011), following the same set-up used in Steig et al. (2015). The fully-coupled simulations were run with both modern and the Pollard and DeConto (2009) 700 ka "collapse" topography, at 0.9°×1.25° resolution with 26 vertical levels in the atmosphere, 1° resolution with 60 vertical levels in the ocean, and full coupling between the

Accepted for publication in *Journal of Climate*. DOI 10.1175/JCLI-D-22-0647.1.

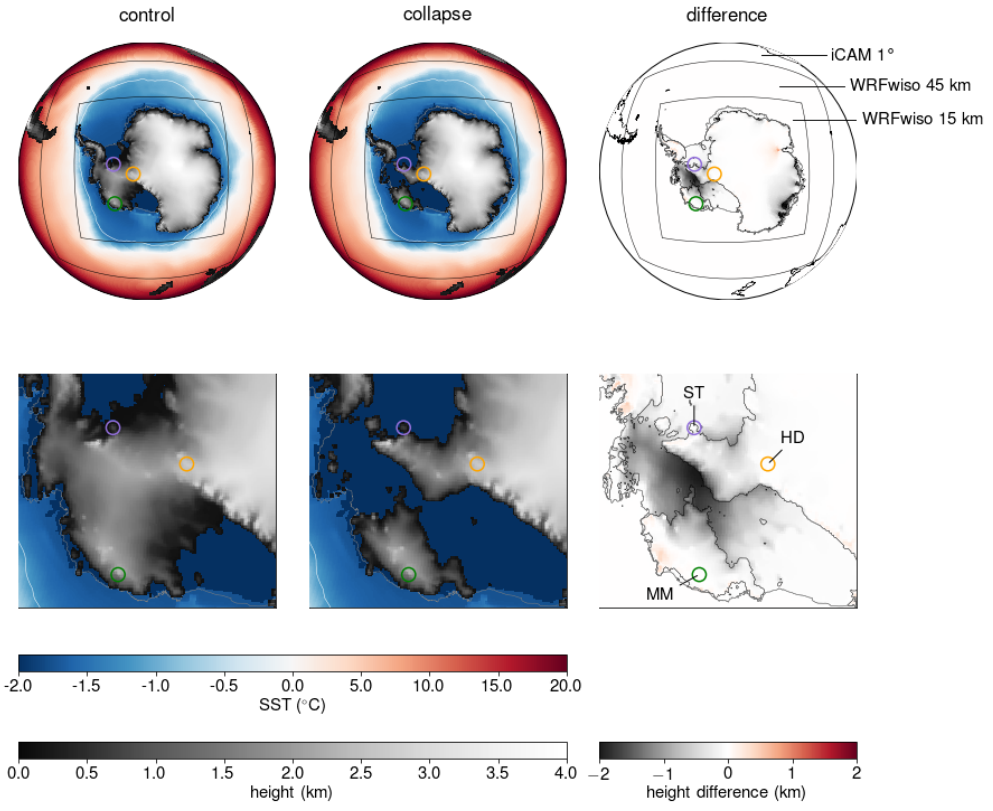

FIG. 1. Sea surface temperature (SST) and Antarctic topography in the WRFwiso simulations, nested within the iCAM simulation. Black lines indicate the boundaries of the WRFwiso domains. The white line corresponds to the sea-ice edge (where sea-ice concentration > 50%). The rightmost panels show the change in topography (*collapse* minus *control*). Orange, purple, and green circles show the locations of Hercules Dome (HD), SkyTrain Ice Rise (ST), and Mount Moulton (MM), respectively. Note the nonlinear color scale for SST.

atmosphere, land, ocean and sea ice components. The simulations were branched from an existing pre-industrial control integration of CCSM4, and run for 300 years. The possible influence of ice-sheet melting is not included – any changes to the ocean in the fully-coupled simulations result solely from the atmospheric and ocean-circulation changes caused by the topography changes. The sea ice and ocean surface conditions from these fully-coupled runs were then used as boundary conditions for the iCAM simulations, using the monthly CCSM4 climatology computed over the last 30 years of each simulation. Note that the fully-coupled simulations did not include isotopes. As in WRFwiso, we set the isotopic composition of the ocean surface to Vienna Standard Mean Ocean Water composition when running iCAM.

Accepted for publication in *Journal of Climate*. DOI 10.1175/JCLI-D-22-0647.1.

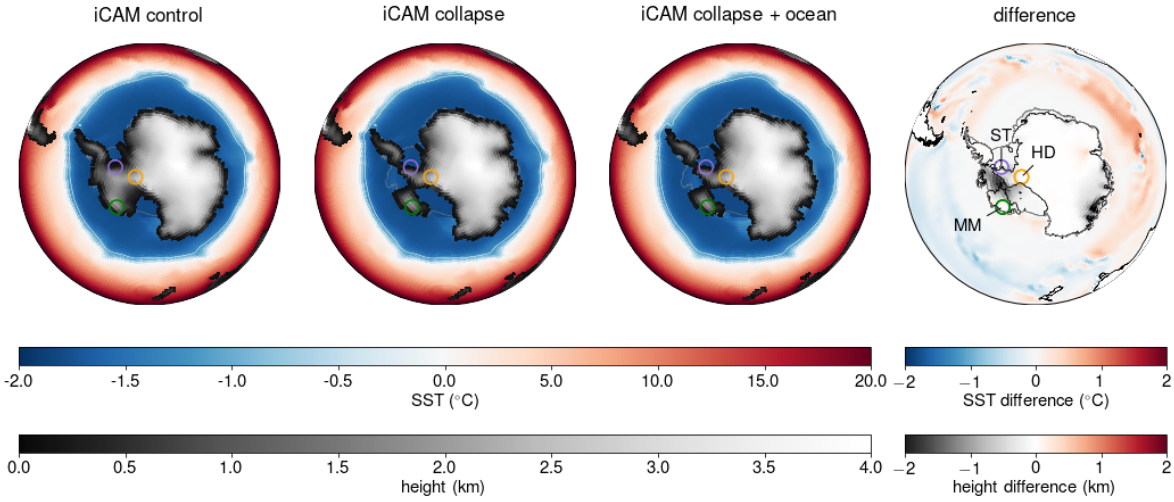

FIG. 2. Sea surface temperature (SST) and Antarctic topography in the iCAM simulations that use boundary conditions from the fully-coupled runs of CCSM4. The white line shows the sea-ice edge (where sea-ice concentration > 50%). The rightmost panel shows the change in topography (*iCAM collapse* minus *iCAM control*) and SST (*iCAM collapse + ocean* minus *iCAM collapse*). Locations of ice cores as in Fig. 1. Note the nonlinear color scale for SST.

Figure 2 illustrates the additional iCAM simulations. *iCAM control* refers to the simulation using modern topography, with pre-industrial ocean surface conditions taken from the fully-coupled control run. *iCAM collapse* uses the lowered ice sheet topography but the same pre-industrial ocean surface conditions. Finally, *iCAM collapse + ocean* uses both lowered ice sheet topography *and* the ocean surface conditions from the fully-coupled collapse simulation with CCSM4.

3. Results

a. Evaluation of WRFwiso (and iCAM)

In Figures 3 and 4, the climatology of precipitation δ^{18}O and d-excess in the *control* simulations of WRFwiso and iCAM are compared with measurements compiled in Masson-Delmotte et al. (2008). We use the measurements only from "traverse", firn cores, and snow pits, because of the high frequency noise in other sample types such as fresh snowfall and the varying time periods covered by ice cores. Both WRFwiso and iCAM nicely capture the spatial δ^{18}O pattern, with high values at the coast of Antarctica and low values further inland (Fig. 3a,b). The d-excess is less well reproduced by the models. In particular the highest values are slightly overestimated by WRFwiso

Accepted for publication in *Journal of Climate*. DOI 10.1175/JCLI-D-22-0647.1.

and underestimated by iCAM (Fig. 3c,d). Nevertheless, the overall spatial pattern is captured by WRFwiso, and to a lesser extent also by iCAM. In terms of Pearson correlation coefficient (R) and root mean square error (RMSE) WRFwiso outperforms iCAM for both δ^{18}O and d-excess (Fig. 4), except for a slightly lower correlation coefficient for δ^{18}O. It is important to note that we would not expect RMSE to be zero even for a perfect representation of the isotope physics, since we are comparing observations with idealized experiments (e.g. we set δ^{18}O and δD for the surface ocean = 0). Rather, we are interested in how well the models capture the spatial pattern, and whether this is improved at higher resolution. Key here is that for both δ^{18}O and d-excess, the WRFwiso results are closer to the 1:1 line than the iCAM results, which is clearly related to the better-resolved topography of the former.

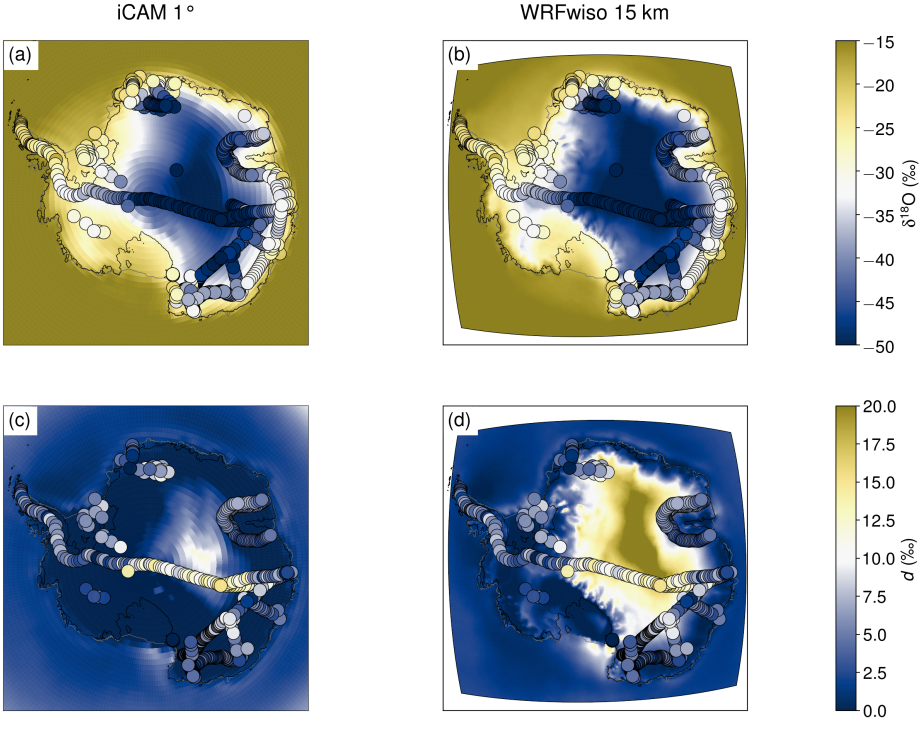

FIG. 3. Comparison of modeled and measured δ^{18}O and d-excess. The shading represents the values simulated by (a,c) iCAM and (b,d) WRFwiso, and the dots show the measurements from Masson-Delmotte et al. (2008).

b. Impact of WAIS collapse

The impact of a collapse of the WAIS, measured as the difference from the control for the simulation that includes lowered West Antarctic topography but no change in ocean surface conditions,

Accepted for publication in *Journal of Climate*. DOI 10.1175/JCLI-D-22-0647.1.

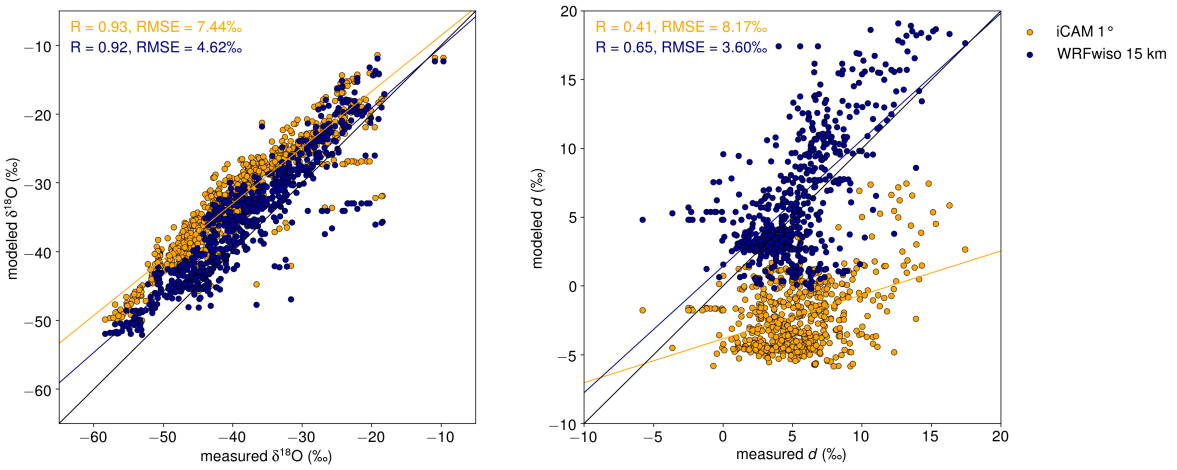

FIG. 4. Modeled and measured δ^{18}O and d-excess at the measurement sites in the data set from Masson-Delmotte et al. (2008). The values from iCAM (orange) and WRFwiso (dark blue) are interpolated linearly to the sites. R is the Pearson correlation coefficient and RMSE is the root mean square error. Colored lines represent the least squares fit to the dots. Black line is the 1:1 line.

is shown in Figure 5 for three different resolutions: the 0.9°×1.25° resolution of iCAM, and the 45 km and 15 km nested WRFwiso domains. Hatching indicates areas where the differences in the annual means of the two simulations are significant at the $p < 0.05$ level, according to a two-sided t-test on the annual means.

In all simulations, a collapse of the WAIS produces a cyclonic wind anomaly over West Antarctica; the same occurs over areas in East Antarctica where the Pollard and DeConto (2009) ice-sheet model simulations also show large ice-sheet elevation changes (Fig. 5a-c). These cyclonic anomalies are a direct result of the expansion of the air column due to a lowering of topography, since potential vorticity conservation causes the relative vorticity to increase in the same direction as the planetary vorticity (i.e., cyclonically). As previously discussed in Steig et al. (2015), this leads to more onshore winds from the Weddell Sea toward West Antarctica, and more offshore winds from West Antarctica toward the Ross Sea, which results in less precipitation over the Transantarctic Mountains and over the Ross Sea, and more precipitation over the Weddell Sea (Fig. 5d-f). Most of East Antarctica receives more precipitation as well. A collapse of the WAIS also leads to higher temperatures across most of Antarctica, and lower temperatures over the Southern Ocean (Fig. 5g-i). Note, again, that the collapse simulations include only topography changes and no

Accepted for publication in *Journal of Climate*. DOI 10.1175/JCLI-D-22-0647.1.

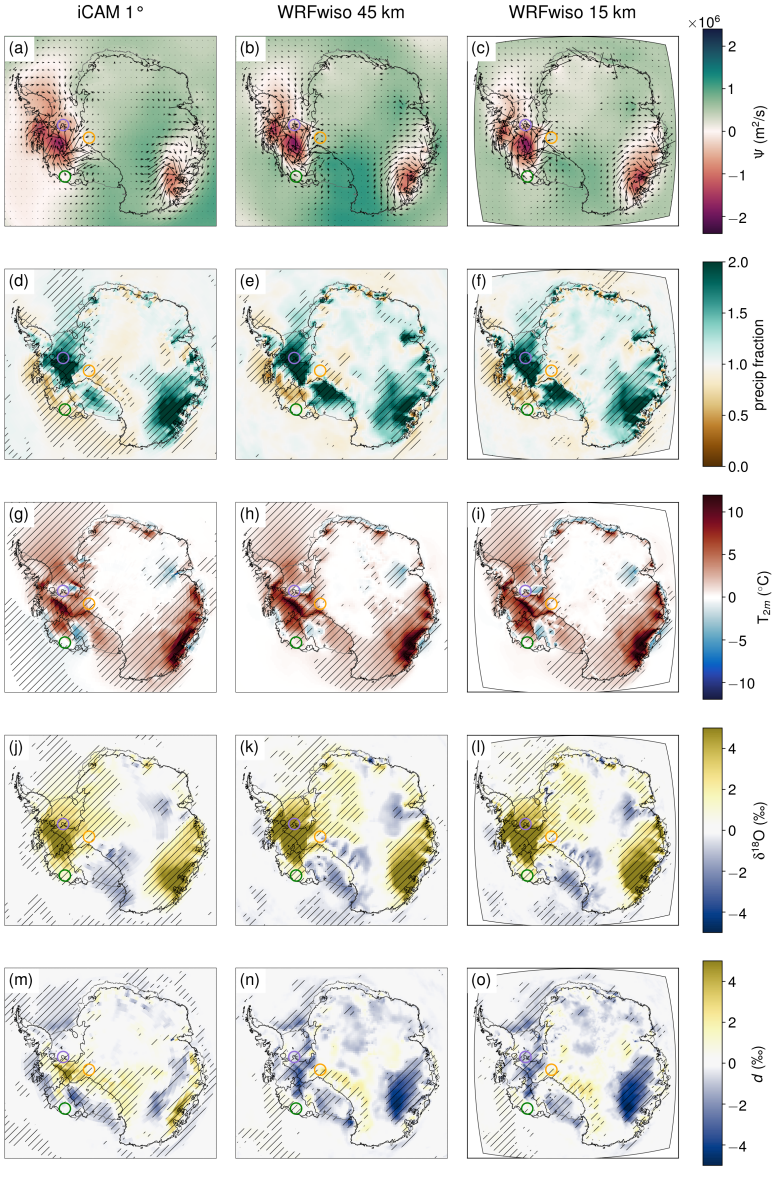

FIG. 5. Impact of WAIS collapse topography as a function of model resolution. The left column shows results from iCAM at 0.9°×1.25° resolution. The middle and right columns show results from WRFwiso for the 45 km and 15 km domains, respectively. Variables shown are (a-c) 10m winds (arrows) and stream function of the nondivergent part of the flow (colors), (d-f) precipitation, (g-i) 2m temperature, (j-l) δ^{18}O, and (m-o) d-excess. The values correspond to the differences (for precipitation, fractional change) between the simulations *collapse* and *control*. In panels d–o, hatching indicates areas where the differences in the annual means are significant at the $p < 0.05$ level. Locations of ice cores as in Fig. 1.

Accepted for publication in *Journal of Climate*. DOI 10.1175/JCLI-D-22-0647.1.

changes to climate forcing (e.g., greenhouse gases and insolation). The higher temperatures in most areas primarily reflect adiabatic warming connected to the lowering of topography, but higher temperatures elsewhere (and lower temperatures in some areas) are the consequence of the circulation changes, as can be seen by comparing temperature to potential temperature (see Supplementary Figure S3). The differences in δ^{18}O follow a combination of the differences in temperature and precipitation. In general, δ^{18}O is lower where temperature and precipitation are lower and vice versa (Fig. 5j-l). The d-excess tends to show a pattern opposite to that of δ^{18}O, but it is not as clearly related to temperature or precipitation (Fig. 5m-o). The results are not meaningfully different if a logarithmic definition for d-excess (Uemura et al. 2012; Dütsch et al. 2017; Markle et al. 2017) is used (see Supplementary Figure S4).

Thanks to the higher resolution, the WRFwiso simulations show more detail and higher variability on small spatial scales than the iCAM-only simulations or previously published results. This is particularly apparent at the locations of the ice-core sites of interest (see Supplementary Figure S5), illustrating the value of high-resolution simulations in regions with fine-scale topographic features. Nevertheless, the overall pattern of the differences between the *collapse* and *control* simulations at different resolutions is very similar.

c. Separate impact of topography and ocean surface conditions

The additional simulations with iCAM, in which we use ocean surface boundary conditions from the fully-coupled runs, allow us to separate the direct impact of topography from the additional impact of changes in ocean surface conditions (which are themselves a consequence of the topography-induced atmospheric circulation changes). In particular, we can isolate the effect of the ocean surface changes by subtracting the *iCAM collapse* simulation from the *iCAM collapse + ocean* simulation. The results (Figure 6) show that while accounting for the changes in ocean surface conditions is important for surface climate variables over the ocean, it has little impact over the Antarctic continent. At most locations on the ice sheet, the difference between the total impact (topography + ocean surface) and the topography-only impact is small. Exceptions to this include lower precipitation, δ^{18}O, and d-excess over some regions of East Antarctica, but there is little impact at the ice-core sites in and adjacent to the WAIS. For this reason, we did not conduct additional WRFwiso simulations using these changed ocean surface boundary conditions. Note

Accepted for publication in *Journal of Climate*. DOI 10.1175/JCLI-D-22-0647.1.

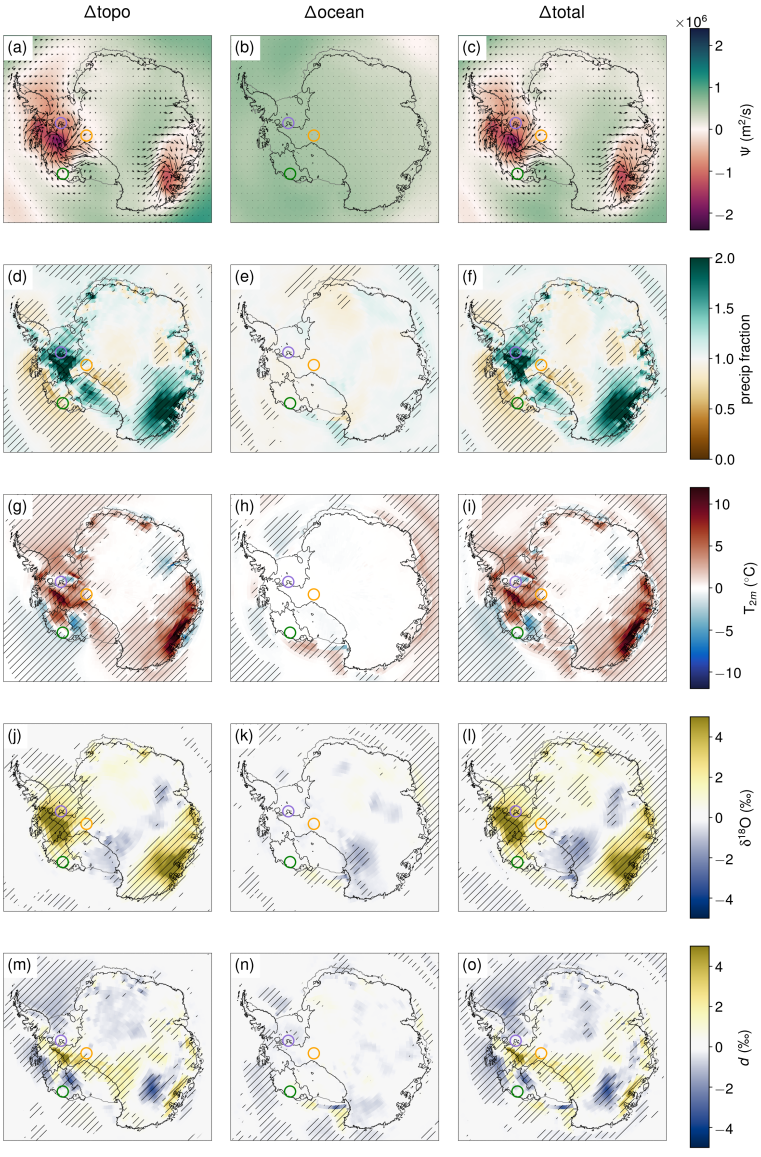

FIG. 6. Impact of differences in topography and ocean surface conditions from the iCAM simulations with ocean surface boundary conditions from the fully-coupled simulations. Shown are (a-c) 10m winds (arrows) and stream function of the nondivergent part of the flow (colors), (d-f) precipitation, (g-i) 2m temperature, (j-l) $\delta^{18}O$, and (m-o) d-excess. The values correspond to the differences (for precipitation, fractional change) between the simulations *iCAM collapse* and *iCAM control* (left), *iCAM collapse* + *ocean* and *iCAM collapse* (middle), and *iCAM collapse* + *ocean* and *iCAM control* (right). In panels d–o, hatching indicates areas where the differences in the annual means are significant at the $p < 0.05$ level. Locations of ice cores as in Fig. 1.

Accepted for publication in *Journal of Climate*. DOI 10.1175/JCLI-D-22-0647.1.

that the impact of topography alone is very similar to that in Figure 5 despite the different ocean surface conditions, which lends additional credibility to these results. An important caveat is that in Victoria Land, which includes the ice-core sites Taylor Dome and Talos Dome, the ocean surface boundary condition changes that result from WAIS topographic changes may have an impact on δ^{18}O and d-excess comparable to that of topography alone.

d. Potential for evidence of WAIS collapse in ice-core records

To further examine the impact of the topographic changes associated with WAIS collapse on water isotope ratios at ice-core sites, we compile the results for each of the WRFwiso grid points within 50 km of each ice-core site at which Eemian ice has been (or could be) obtained. Figure 7 shows the results as violin plots, illustrating the mean and spatial variability for Hercules Dome, SkyTrain Ice Rise, and Mount Moulton. We show the same for additional locations in Supplementary Figure S6. We also show the changes in topography at each of these locations, because this has a direct affect on the surface climate, including the isotopic concentrations, through the temperature lapse rate. These calculations provide a measure for the spatial uncertainty that would need to be kept in mind when applying our results to actual measurements. In particular, our results suggest that the location of the prospective Hercules Dome ice core lies near the boundary between regions with higher and lower δ^{18}O resulting from WAIS collapse (cf. Figure 5j-l). Hercules Dome covers a fairly small area of $\sim$ 50×100 km (Jacobel et al. 2005; Fudge et al. 2022). While the mean δ^{18}O anomaly at Hercules Dome is greater than 1‰, the spatial variability is almost as large. On the other hand, the d-excess anomaly at Hercules Dome is positive over the entire region, suggesting that d-excess would be a more robust signal for a WAIS collapse at this location. We find that at Mount Moulton, the anomaly in δ^{18}O is comparable to that at Hercules Dome. Critically, the mean simulated δ^{18}O anomaly at Mount Moulton is positive, whereas earlier results from Steig et al. (2015) conducted at much lower (2.5°) resolution indicated a negative anomaly. In contrast, at SkyTrain Ice Rise the δ^{18}O anomaly is much larger than at either Hercules Dome or Mount Moulton, and the spatial variability is smaller. Although part of the δ^{18}O anomaly at SkyTrain is almost certainly owing to the ~40 m lowering of the local topography in our simulations, this can account for only about 20% of the magnitude (see Discussion, next section). Overall, these results show that, for our particular simulations, the most robust isotopic signals from a WAIS collapse

Accepted for publication in *Journal of Climate*. DOI 10.1175/JCLI-D-22-0647.1.

are elevated δ^{18}O at SkyTrain Ice Rise, and elevated d-excess at Hercules Dome. In the Discussion which follows we consider the implications of these results for the interpretation and analysis of existing and potential future ice-core records.

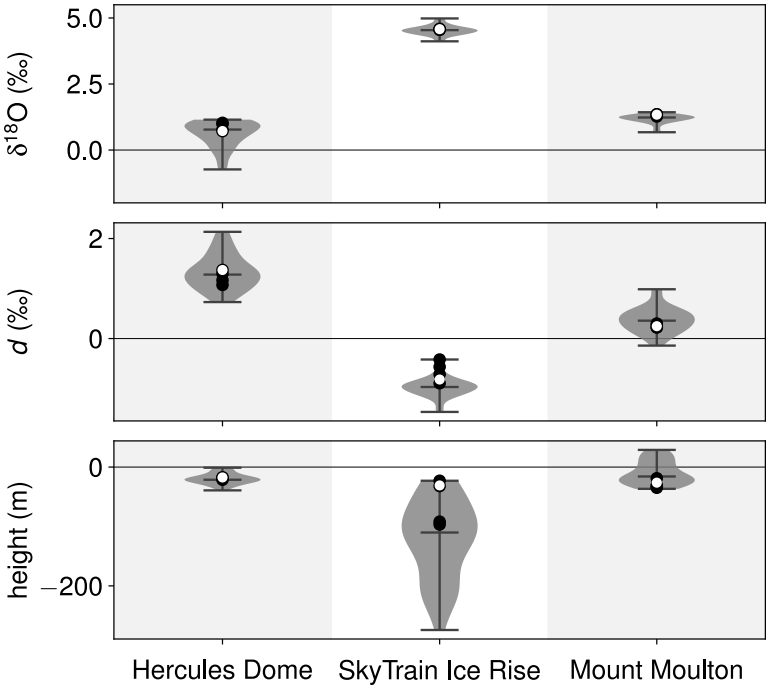

FIG. 7. Violin plot showing the variability of change in (a) δ^{18}O and (b) d-excess in precipitation within 50 km of the ice-core sites Hercules Dome, SkyTrain Ice Rise, and Mount Moulton, between the *collapse* and *control* WRFwiso 15 km simulations. The width of each violin corresponds to the frequency of data points. White dots show the values interpolated to the latitude and longitude of the ice-core sites. Black dots show the values at the four surrounding grid points. The horizontal bars show the maximum, median, and minimum values.

4. Discussion

The high-resolution simulations conducted with WRFwiso agree well with previous work that has examined the impact of topographic changes on Antarctic climate using lower-resolution models (Steig et al. 2015; Holloway et al. 2016; Goursaud et al. 2021). Our results support the conclusion that a collapse of the West Antarctic Ice Sheet (WAIS) would cause substantial changes in surface climate and isotopes in precipitation, not only directly where the topography has lowered, but

Accepted for publication in *Journal of Climate*. DOI 10.1175/JCLI-D-22-0647.1.

also in adjacent areas, owing to changes in atmospheric circulation. Our results also clarify some questions that this earlier work has raised. In particular, we find that the spatial variability of the response in areas of mountainous topography is great enough that lower-resolution simulations should be treated with caution when considering applications to specific ice-core locations. At Mount Moulton, which Steig et al. (2015) had suggested could provide definitive evidence of WAIS collapse, the magnitude and sign of the local climate response to lowered WAIS topography is ambiguous. However, at other key ice-core locations of interest for potentially detecting evidence of past changes in the WAIS, the response appears to be more robust. Specifically, for the particular configuration of WAIS collapse topography that we use in our simulations, the signatures of WAIS collapse in both δ^{18}O and d-excess in precipitation (as well as in precipitation rate and surface temperature) are sufficiently large and spatially uniform to be detectable at ice-core sites including SkyTrain Ice Rise and Hercules Dome.

An ice core was recently obtained at SkyTrain Ice Rise that apparently recovered Eemian ice (Mulvaney et al. 2021), and an ice core is currently planned for the Hercules Dome site some time this decade, which is also expected to recover Eemian ice (Fudge et al. 2022). Given the potential utility of such records for constraining the timing and magnitude of WAIS collapse, if it occurred during that time period, it is important to understand the origin of the signals we observe in our simulation for these locations. For δ^{18}O, temperature, and precipitation, interpretation is straightforward: the lowered WAIS topography causes a large scale circulation anomaly that brings more warm, moist air across the Weddell Sea region, affecting SkyTrain Ice Rise and Hercules Dome. The impact is much larger at SkyTrain, owing to its relatively low elevation (780 m above sea level) and its location at the edge of the Ronne-Filchner ice shelf in the Weddell Sea, as is evident in the large wind and stream function anomalies shown in Figure 5 and Supplementary Figure S5. At this location, the sign of the δ^{18}O, precipitation rate, and temperature anomalies are all positive, and quite spatially homogeneous at all model resolutions we considered. The simulated δ^{18}O response at SkyTrain Ice Rise is about 4.6 ‰. Observed scaling between local elevation and δ^{18}O is about 10 ‰/km (e.g., Fudge et al. 2020), while SkyTrain Ice Rise is lowered by less than 50 m in the "collapse" topography we use; hence, an anomaly of at least 4 ‰ reflects atmospheric circulation change associated with WAIS collapse. This is a very strong anomaly,

Accepted for publication in *Journal of Climate*. DOI 10.1175/JCLI-D-22-0647.1.

more than one half the magnitude of the full glacial-interglacial δ^{18}O change in Antarctic ice cores (e.g., Landais et al. 2021; Kahle et al. 2021).

At Hercules Dome, both δ^{18}O and temperature anomalies are positive over the relatively small area under consideration for an ice-core record, but this result may be sensitive to the actual pattern of WAIS elevation change. There is an accumulation gradient across Hercules Dome today, with lower precipitation to the east (toward the top of the map in the figures), and higher precipitation to the west, which reflects the greater propensity of storms crossing the WAIS to reach Hercules Dome from the west (from the direction of the Ross Sea, e.g., Nicolas and Bromwich 2011). When WAIS collapse occurs in our simulations, more storms reach Hercules Dome from the east (i.e., from the direction of the Weddell Sea). This suggests that the spatial gradient in precipitation would change in response to the topographic change, and the sign of the local change preserved in an ice-core record could depend on the details of the topographic change. Furthermore, the sign of the simulated local response in precipitation rate at Hercules Dome varies from negative to positive with increasing model resolution (Supplementary Figure S5). Similarly, the sign of the local change would depend on the specific location of the ice core. The potential may exist to examine changes in the precipitation gradient in the past using ice-penetrating radar observations (e.g., Waddington et al. 2007).

In contrast with δ^{18}O, the d-excess signal is more robust at Hercules Dome than at SkyTrain Ice Rise. The d-excess signal is evidently associated with the change in orographic gradient between modern and collapse topography, owing to the strong fractionation that occurs when moisture-bearing air masses traverse the steep topography of the Transantarctic Mountain front. Indeed, there is a statistically significant d-excess increase along the entire Transantarctic Mountains between Hercules Dome and Victoria Land, at all model resolutions. As would be expected if this pattern is associated with orographic precipitation (e.g., Guan et al. 2009; Galewsky 2009), the anomaly becomes narrower (more closely associated with the mountain front) at finer model resolution. Even in the simulation with the finest model resolution (WRFwiso 15 km), Hercules Dome lies well within the area of the d-excess anomaly (see Figure 5 and Supplementary Figure S5). The spatial extent of the anomaly relative to the relatively small area of Hercules Dome is even more evident in the logarithmic formulation of d-excess (Uemura et al. 2012; Markle et al. 2017) (see

Accepted for publication in *Journal of Climate*. DOI 10.1175/JCLI-D-22-0647.1.

Supplementary Figure S4). Moreover, the magnitude of this anomaly is large; amounting to about 20 to 50 % of the typical glacial-interglacial change in Antarctic ice cores (Markle and Steig 2022).

The change in orographic gradient may also explain the d-excess anomalies at Talos Dome and Taylor Dome (Supplementary Figure S6). Indeed, the d-excess anomalies at Talos and Taylor Dome in our simulations are almost as large as that at Hercules Dome. It is of interest to note that data from the Talos Dome ice core (Crotti et al. 2022) also shows a positive anomaly in d-excess compared with some other East Antarctic ice cores. For example, the last-interglacial peak *vs.* Holocene difference at Talos Dome is about 1.5 ‰, while it is close to zero in EPICA Dronning Maud Land (EDML) (Stenni et al. 2010), consistent with our simulations. (Note that d-excess data for Taylor Dome are not available for this time period). On the other hand, while the EPICA Dome C ice core (EDC) observations show a positive d-excess anomaly (Stenni et al. 2010), our simulations show a negative anomaly, though the latter is clearly related to topographic change in East Antarctica. Talos Dome also has the smallest δ^{18}O peak during the last interglacial peak of all existing East Antarctic cores (Masson-Delmotte et al. 2011; Steig et al. 2015), consistent with our simulations. Such simple comparisons between our results and ice core data should be treated with caution, because changes in climate boundary conditions could have a comparable influence, particularly on d-excess, to the impact of the topographic changes we consider here.

Our simulations consider *only* the direct and indirect effects of topographic change associated with possible WAIS collapse, and do not take into account climate changes that would have led to WAIS collapse in the first place. As noted in the Methods, we do not change CO_2, orbital parameters, or other climate forcings. We would expect the climate response to such forcings to be relatively spatially uniform (e.g., Watanabe et al. 2003), and our findings thus provide an estimate of the relative anomalies expected as a result of topographic change. For example, during the peak of the Eemian interglacial, ice cores from the East Antarctic plateau are about 1 ‰ enriched in δ^{18}O relative to their Holocene means (Masson-Delmotte et al. 2011; Steig et al. 2015). Such locations, far from West Antarctica, would not be significantly affected by WAIS topographic changes. If the WAIS collapsed during the Eemian, in a configuration similar to what we have used in our simulations, then we would expect a relative δ^{18}O enrichment at Hercules Dome and SkyTrain Ice Rise of about 1 ‰ and 4 ‰, respectively, in comparison with East Antarctic cores.

Accepted for publication in *Journal of Climate*. DOI 10.1175/JCLI-D-22-0647.1.

The use of ice cores from the East Antarctic plateau as reference points implicitly assumes either that there has been no local elevation change, or that it can be estimated and accounted for. The additional iCAM simulation (*collapse G21*), for which we used the collapse topography from Golledge et al. (2021) instead of Pollard and DeConto (2009), provides one measure of the sensitivity of our results to the topographic configuration. In Supplementary Figure S7, the wind, precipitation, temperature, δ^{18}O, and d-excess anomalies in *collapse G21* are compared to *collapse*. In *collapse G21* the differences in East Antarctica are smaller than in *collapse*, because the topographic change in East Antarctica is smaller. In *collapse*, the EDC site is affected by both local and regional elevation changes, with commensurately large isotopic anomalies (Supplementary Figure S6); these are reduced in *collapse G21*. In contrast, the location of Dome Fuji shows no significant change in either topography, suggesting that it may provide the better estimate of the background (i.e., unaffected by topographic change) response to climate forcing.

The differences in West Antarctica and at Hercules Dome are very similar in *collapse G21* and *collapse*, suggesting that these patterns are quite robust across different topographic configurations. Results for SkyTrain ice rise and Hercules Dome are essentially unchanged (Supplementary Figure S7). The same d-excess anomaly pattern along and inland of the Transantarctic mountains and in Victoria Land, where Talos and Taylor Dome are located, appears in both sets of simulations, supporting the robustness of the signal at these sites. For Hercules Dome, it will be important to further explore the relationship between the spatial pattern of the isotopic signal and the spatial gradient in accumulation, which may change in response to topographic changes. Simulations that include a fuller range of possible topographies and climate scenarios will need to be conducted to make full use of the ice core data in assessing Antarctic ice sheet changes.

5. Conclusions

We performed high-resolution simulations with a water-isotope-enabled version of the Weather Research and Forecasting (WRF) model to quantify the impact of a WAIS collapse on circulation, precipitation, temperature, and water isotopes (δ^{18}O and d-excess). In particular we focused on three ice-core sites in or adjacent to West Antarctica: Mount Moulton Blue Ice Area, SkyTrain Ice Rise, and Hercules Dome. Our results largely support previous work, showing that ice-core records could potentially constrain the size of the WAIS in the past. A collapse of the WAIS

Accepted for publication in *Journal of Climate*. DOI 10.1175/JCLI-D-22-0647.1.

has a large impact on Antarctic climate: it leads to a cyclonic atmospheric circulation anomaly over West Antarctica, more precipitation in the Weddell Sector and less precipitation in the Ross Sector, and warmer surface temperatures across most of Antarctica. WAIS collapse also impacts ocean circulation, potentially changing sea surface temperature and sea ice distribution; however, the additional effect of the ocean surface changes on the surface climate over the ice sheet is relatively small: the direct effects of topography and atmospheric circulation change dominate. These changes will be reflected in the isotopic composition of precipitation as recorded in ice cores. Because the spatial variability of the response can be large, particularly in mountainous regions, some ice-core locations are more sensitive, and will be better indicators of WAIS topography change, than others. The Mount Moulton site in West Antarctic is probably a less reliable indicator than originally suggested by Steig et al. (2015). Elevated temperature, precipitation and δ^{18}O at SkyTrain Ice Rise, and higher δ^{18}O and d-excess at Hercules Dome are more consistent across model resolutions, and are likely to be more robust signals of WAIS collapse.

Accepted for publication in *Journal of Climate*. DOI 10.1175/JCLI-D-22-0647.1.

Acknowledgments. We thank David Reusch, Jordan Powers and Kevin Manning for helpful advice on configuring WRF simulations over Antarctica. We acknowledge high-performance computing support from Cheyenne (doi:10.5065/D6RX99HX) provided by NCAR's Computational and Information Systems Laboratory, sponsored by the National Science Foundation. We also acknowledge support from NSF grant OPP-1602435. Early work on WRFwiso by PNB was supported by NSF grant AGS-1260368. We thank Kurt Cuffey and two anonymous reviewers for their helpful comments, which improved our manuscript.

Data availability statement. iCESM (including iCAM and iCLM) is publicly accessible online (`https://github.com/NCAR/iCESM1.2`). WRFwiso is available at `https://github.com/pblossey/WRFwiso`. Model output data and scripts to create the figures are available at `https://doi.org/10.5281/zenodo.7007864`.

References

Bamber, J. L., R. E. Riva, B. L. Vermeersen, and A. M. LeBrocq, 2009: Reassessment of the potential sea-level rise from a collapse of the West Antarctic Ice Sheet. *Science*, **324 (5929)**, 901–903, https://doi.org/10.1126/science.1169335.

Bazin, L., and Coauthors, 2013: An optimized multi-proxy, multi-site Antarctic ice and gas orbital chronology (AICC2012): 120–800 ka. *Climate of the Past*, **9 (4)**, 1715–1731, https://doi.org/10.5194/cp-9-1715-2013.

Blossey, P. N., Z. Kuang, and D. M. Romps, 2010: Isotopic composition of water in the tropical tropopause layer in cloud-resolving simulations of an idealized tropical circulation. *Journal of Geophysical Research: Atmospheres*, **115 (D24)**, https://doi.org/10.1029/2010JD014554.

Brady, E., and Coauthors, 2019: The connected isotopic water cycle in the Community Earth System Model version 1. *J. Adv. Model. Earth Sy.*, **11 (8)**, 2547–2566, https://doi.org/10.1029/2019MS001663.

Bromwich, D. H., F. O. Otieno, K. M. Hines, K. W. Manning, and E. Shilo, 2013: Comprehensive evaluation of polar weather research and forecasting model performance in the Antarctic. *Journal of Geophysical Research: Atmospheres*, **118 (2)**, 274–292.

Accepted for publication in *Journal of Climate*. DOI 10.1175/JCLI-D-22-0647.1.

Crotti, I., and Coauthors, 2022: Wilkes subglacial basin ice sheet response to Southern Ocean warming during late Pleistocene interglacials. *Nat. Commun.*, **13 (5328)**, https://doi.org/doi.org/10.1038/s41467-022-32847-3.

Dütsch, M., P. N. Blossey, E. J. Steig, and J. M. Nusbaumer, 2019: Non-equilibrium fractionation during ice cloud formation in iCAM5: evaluating the common parameterization of supersaturation as a linear function of temperature. *J. Adv. Model. Earth Sy.*, **11**, 377–3793, https://doi.org/10.1029/2019MS001764.

Dütsch, M., S. Pfahl, and H. Sodemann, 2017: The impact of nonequilibrium and equilibrium fractionation on two different deuterium excess definitions. *Journal of Geophysical Research: Atmospheres*, **122 (23)**, 12,732–12,746, https://doi.org/10.1002/2017JD027085.

Dutton, A., and K. Lambeck, 2012: Ice volume and sea level during the last interglacial. *Science*, **337 (6091)**, 216–219, https://doi.org/10.1126/science.1205749.

Dyer, B., J. Austermann, W. J. D'Andrea, R. C. Creel, M. R. Sandstrom, M. Cashman, A. Rovere, and M. E. Raymo, 2021: Sea-level trends across the bahamas constrain peak last interglacial ice melt. *Proceedings of the National Academy of Sciences*, **118 (33)**, e2026839 118, https://doi.org/10.1073/pnas.2026839118.

Fischer, H., and Coauthors, 2018: Palaeoclimate constraints on the impact of 2 °C anthropogenic warming and beyond. *Nature Geoscience*, **11 (7)**, 474–485, https://doi.org/10.1038/s41561-018-0146-0.

Fudge, T., D. Lilien, M. Koutnik, H. Conway, C. Stevens, E. Waddington, E. Steig, and A. Schauer, 2020: Advection impact on the South Pole Ice Core. *Climate of the Past*, **16**, 819–832, https://doi.org/10.5194/cp-16-819-2020.

Fudge, T., and Coauthors, 2022: A site for deep ice coring at West Hercules Dome: results from ground-based geophysics and modeling. *Journal of Glaciology*, 1–13, https://doi.org/10.1017/jog.2022.80.

Galewsky, J., 2009: Orographic precipitation isotopic ratios in stratified atmospheric flows: Implications for paleoelevation studies. *Geology*, **37 (9)**, 791–794, https://doi.org/10.1130/G30008A.1.

Accepted for publication in *Journal of Climate*. DOI 10.1175/JCLI-D-22-0647.1.

Gent, P. R., and Coauthors, 2011: The Community Climate System Model Version 4. *J. Climate*, **24 (19)**, 4973–4991, https://doi.org/10.1175/2011JCLI4083.1.

Golledge, N. R., and Coauthors, 2021: Retreat of the Antarctic Ice Sheet during the Last Interglaciation and implications for future change. *Geophysical Research Letters*, **48 (17)**, e2021GL094 513, https://doi.org/10.1029/2021GL094513.

Goursaud, S., M. D. Holloway, L. C. Sime, E. Wolff, P. J. Valdes, E. J. Steig, and A. G. Pauling, 2021: Antarctic Ice Sheet elevation impacts on water isotope records during the Last Interglacial. *Geophys. Res. Lett*, **48 (6)**, e2020GL091 412, https://doi.org/10.1029/2020GL091412.

Guan, H., C. T. Simmons, and A. J. Love, 2009: Orographic controls on rain water isotope distribution in the mount lofty ranges of south australia. *Journal of Hydrology*, **374 (3)**, 255–264, https://doi.org/https://doi.org/10.1016/j.jhydrol.2009.06.018.

Hoffmann, G., M. Werner, and M. Heimann, 1998: Water isotope module of the ECHAM atmospheric general circulation model: A study on timescales from days to several years. *J. Geophys. Res.*, **103**, 16 871–16 896, https://doi.org/10.1029/98JD00423.

Holden, P. B., N. R. Edwards, E. W. Wolff, N. J. Lang, J. S. Singarayer, P. J. Valdes, and T. F. Stocker, 2010: Interhemispheric coupling, the West Antarctic ice sheet and warm Antarctic interglacials. *Clim. Past*, **6 (4)**, 431–443, https://doi.org/10.5194/cp-6-431-2010.

Holloway, M. D., L. C. Sime, J. S. Singarayer, J. C. Tindall, P. Bunch, and P. J. Valdes, 2016: Antarctic last interglacial isotope peak in response to sea ice retreat not ice-sheet collapse. *Nat. Commun.*, **7**, 12 293, https://doi.org/10.1038/ncomms12293.

Hurrell, J. W., J. J. Hack, D. Shea, J. M. Caron, and J. Rosinski, 2008: A new sea surface temperature and sea ice boundary dataset for the Community Atmosphere Model. *Journal of Climate*, **21 (19)**, 5145–5153, https://doi.org/10.1175/2008JCLI2292.1.

Iacono, M. J., J. S. Delamere, E. J. Mlawer, M. W. Shephard, S. A. Clough, and W. D. Collins, 2008: Radiative forcing by long-lived greenhouse gases: Calculations with the AER radiative transfer models. *Journal of Geophysical Research: Atmospheres*, **113 (D13)**, https://doi.org/https://doi.org/10.1029/2008JD009944.

Accepted for publication in *Journal of Climate*. DOI 10.1175/JCLI-D-22-0647.1.

Jacobel, R. W., B. C. Welch, E. J. Steig, and D. P. Schneider, 2005: Glaciological and climatic significance of hercules dome, antarctica: An optimal site for deep ice core drilling. *Journal of Geophysical Research: Earth Surface*, **110 (F1)**, https://doi.org/https://doi.org/10.1029/2004JF000188.

Janjic, Z., 1996: The surface layer parameterization in the NCEP Eta Model. *World Meteorological Organization-Publications-WMO TD*, 4–16.

Janjić, Z. I., 2001: Nonsingular implementation of the Mellor-Yamada level 2.5 scheme in the NCEP Meso model. Office note, #437, National Centers for Environmental Prediction (U.S.). URL https://repository.library.noaa.gov/view/noaa/11409.

Justino, F., A. Silva, M. Pereira, F. Stordal, D. Lindemann, and F. Kucharski, 2015: The large-scale climate in response to the retreat of the West Antarctic Ice Sheet. *Journal of Climate*, **28 (2)**, 637–650, https://doi.org/10.1175/JCLI-D-14-00284.1.

Kahle, E. C., and Coauthors, 2021: Reconstruction of temperature, accumulation Rate, and layer thinning from an ice core at South Pole, using a statistical inverse method. *Journal of Geophysical Research: Atmospheres*, **126 (13)**, e2020JD033 300, https://doi.org/10.1029/2020JD033300.

Kopp, R. E., F. J. Simons, J. X. Mitrovica, A. C. Maloof, and M. Oppenheimer, 2009: Probabilistic assessment of sea level during the last interglacial stage. *Nature*, **462 (7275)**, 863–867, https://doi.org/10.1038/nature08686.

Korotkikh, E. V., P. A. Mayewski, M. J. Handley, S. B. Sneed, D. S. Introne, A. V. Kurbatov, N. W. Dunbar, and W. C. McIntosh, 2011: The last interglacial as represented in the glaciochemical record from Mount Moulton Blue Ice Area, West Antarctica. *Quat. Sci. Rev.*, **30 (15-16)**, 1940–1947, https://doi.org/10.1016/j.quascirev.2011.04.020.

Landais, A., and Coauthors, 2021: Interglacial Antarctic–Southern Ocean climate decoupling due to moisture source area shifts. *Nature Geoscience*, **14 (12)**, 918–923, https://doi.org/10.1038/s41561-021-00856-4.

Majoube, M., 1970: Fractionation factor of ^{18}O between water vapour and ice. *Nature*, **226 (5252)**, 1242–1242.

Accepted for publication in *Journal of Climate*. DOI 10.1175/JCLI-D-22-0647.1.

Majoube, M., 1971: Fractionnement en oxygène 18 et en deutérium entre l'eau et sa vapeur. *J. Chim. Phys.*, **68 (4)**, 625–636.

Markle, B. R., and E. J. Steig, 2022: Improving temperature reconstructions from ice-core water-isotope records. *Clim. Past.*, **18**, 1321–1368, https://doi.org/10.5194/cp-18-1321-2022.

Markle, B. R., and Coauthors, 2017: Global atmospheric teleconnections during Dansgaard–Oeschger events. *Nature Geoscienc*, **10 (1)**, 36–40, https://doi.org/10.1038/ngeo2848.

Masson-Delmotte, V., and Coauthors, 2008: A review of Antarctic surface snow isotopic composition: Observations, atmospheric circulation, and isotopic modeling. *Journal of Climate*, **21 (13)**, 3359–3387, https://doi.org/10.1175/2007JCLI2139.1.

Masson-Delmotte, V., and Coauthors, 2011: A comparison of the present and last interglacial periods in six Antarctic ice cores. *Clim. Past*, **7 (2)**, 397–423, https://doi.org/10.5194/cp-7-397-2011.

McKay, N. P., J. T. Overpeck, and B. L. Otto-Bliesner, 2011: The role of ocean thermal expansion in Last Interglacial sea level rise. *Geophys. Res. Lett.*, **38 (14)**, https://doi.org/10.1029/2011GL048280.

Mercer, J., 1978: West Antarctic ice sheet and CO2 greenhouse effect: a threat of disaster. *Nature*, **271**, 321–325, https://doi.org/10.1038/271321a0.

Merlivat, L., and J. Jouzel, 1979: Global climatic interpretation of the deuterium-oxygen 18 relationship for precipitation. *Journal of Geophysical Research: Oceans*, **84 (C8)**, 5029–5033.

Merlivat, L., and G. Nief, 1967: Fractionnement isotopique lors des changements d'état solide-vapeur et liquide-vapeur de l'eau à des températures inférieures à 0°c. *Tellus*, **19 (1)**, 122–127.

Mlawer, E. J., S. J. Taubman, P. D. Brown, M. J. Iacono, and S. A. Clough, 1997: Radiative tranfer for inhomogeneous atmospheres: RRTM, a validated correlated-k model for the longwave. *J. Geophys. Res.*, **102**, 16 663–16 682, https://doi.org/https://doi.org/10.1029/97JD00237.

Moore, M., P. Blossey, A. Muhlbauer, and Z. Kuang, 2016: Microphysical controls on the isotopic composition of wintertime orographic precipitation. *Journal of Geophysical Research: Atmospheres*, **121 (12)**, 7235–7253.

Accepted for publication in *Journal of Climate*. DOI 10.1175/JCLI-D-22-0647.1.

Mulvaney, R., and Coauthors, 2021: Ice drilling on Skytrain Ice Rise and Sherman Island, Antarctica. *Annals of Glaciology*, **62 (85-86)**, 311–323.

Nicolas, J. P., and D. H. Bromwich, 2011: Climate of West Antarctica and influence of marine air intrusions. *Journal of Climate*, **24 (1)**, 49–67, https://doi.org/10.1175/2010JCLI3522.1.

Nusbaumer, J., T. E. Wong, C. Bardeen, and D. Noone, 2017: Evaluating hydrological processes in the Community Atmosphere Model Version 5 (CAM5) using stable isotope ratios of water. *J. Adv. Model. Earth Sy.*, **9 (2)**, 949–977, https://doi.org/10.1002/2016MS000839.

Otto-Bliesner, B., N. Rosenbloom, E. Stone, N. McKay, D. Lunt, E. Brady, and J. Overpeck, 2013: How warm was the last interglacial? New model–data comparisons. *Philos. Trans. R. Soc. London, Ser. A*, **371**, 1–20, https://doi.org/10.1098/rsta.2013.0097.

Park, S.-H., J. B. Klemp, and J.-H. Kim, 2019: Hybrid mass coordinate in wrf-arw and its impact on upper-level turbulence forecasting. *Monthly Weather Review*, **147 (3)**, 971–985.

Pollard, D., and R. M. DeConto, 2009: Modelling West Antarctic ice sheet growth and collapse through the past five million years. *Nature*, **458 (7236)**, 329–332, https://doi.org/10.1038/nature07809.

Popp, T. J., 2008: The speed and timing of climate change: Detailed ice core stable isotope records from NorthGRIP, Greenland and Mt. Moulton, West Antarctica. Ph.D. thesis, University of Colorado at Boulder.

Schaefer, J. M., and Coauthors, 2016: Greenland was nearly ice-free for extended periods during the Pleistocene. *Nature*, **540 (7632)**, 252–255, https://doi.org/10.1038/nature20146.

Scherer, R. P., A. Aldahan, S. Tulaczyk, G. Possnert, H. Engelhardt, and B. Kamb, 1998: Pleistocene collapse of the West Antarctic ice sheet. *Science*, **281 (5373)**, 82–85, https://doi.org/10.1126/science.281.5373.82.

Skamarock, W. C., and J. B. Klemp, 2008: A time-split nonhydrostatic atmospheric model for weather research and forecasting applications. *Journal of computational physics*, **227 (7)**, 3465–3485, https://doi.org/10.1016/j.jcp.2007.01.037.

Accepted for publication in *Journal of Climate*. DOI 10.1175/JCLI-D-22-0647.1.

Spector, P., J. Stone, D. Pollard, T. Hillebrand, C. Lewis, and J. Gombiner, 2018: West Antarctic sites for subglacial drilling to test for past ice-sheet collapse. *Cryosphere*, **12 (8)**, 2741–2757, https://doi.org/10.5194/tc-12-2741-2018.

Steig, E. J., K. Huybers, H. A. Singh, N. J. Steiger, Q. Ding, D. M. W. Frierson, T. Popp, and J. W. C. White, 2015: Influence of West Antarctic ice sheet collapse on Antarctic surface climate. *Geophys. Res. Lett.*, **42 (12)**, 4862–4868, https://doi.org/10.1002/2015GL063861.

Stenni, B., and Coauthors, 2010: The deuterium excess records of epica dome c and dronning maud land ice cores (east antarctica). *Quaternary Science Reviews*, **29 (1)**, 146–159, https://doi.org/10.1016/j.quascirev.2009.10.009, climate of the Last Million Years: New Insights from EPICA and Other Records.

Thompson, G., P. R. Field, R. M. Rasmussen, and W. D. Hall, 2008: Explicit forecasts of winter precipitation using an improved bulk microphysics scheme. part ii: Implementation of a new snow parameterization. *Monthly Weather Review*, **136 (12)**, 5095–5115.

Tindall, J. C., P. J. Valdes, and L. C. Sime, 2009: Stable water isotopes in HadCM3: Isotopic signature of El Niño–Southern Oscillation and the tropical amount effect. *J. Geophys. Res. Atmos.*, **114**, D04 111, https://doi.org/10.1029/2008JD010825.

Turney, C. S. M., and R. T. Jones, 2010: Does the Agulhas Current amplify global temperatures during super-interglacials? *J. Quaternary Sci.*, **25 (6)**, 839–843, https://doi.org/10.1002/jqs.1423.

Uemura, R., V. Masson-Delmotte, J. Jouzel, A. Landais, H. Motoyama, and B. Stenni, 2012: Ranges of moisture-source temperature estimated from antarctic ice cores stable isotope records over glacial–interglacial cycles. *Climate of the Past*, **8 (3)**, 1109–1125, https://doi.org/10.5194/cp-8-1109-2012.

Veres, D., and Coauthors, 2013: The antarctic ice core chronology (aicc2012): an optimized multi-parameter and multi-site dating approach for the last 120 thousand years. *Climate of the Past*, **9 (4)**, 1733–1748, https://doi.org/10.5194/cp-9-1733-2013.

Accepted for publication in *Journal of Climate*. DOI 10.1175/JCLI-D-22-0647.1.

Waddington, E. D., T. A. Neumann, M. R. Koutnik, H.-P. Marshall, and D. L. Morse, 2007: Inference of accumulation-rate patterns from deep layers in glaciers and ice sheets. *Journal of Glaciology*, **53 (183)**, 694–712.

Wahl, S., H. C. Steen-Larsen, J. Reuder, and M. Hörhold, 2021: Quantifying the stable water isotopologue exchange between the snow surface and lower atmosphere by direct flux measurements. *Journal of Geophysical Research: Atmospheres*, **126 (13)**, e2020JD034 400, https://doi.org/10.1029/2020JD034400.

WAIS Divide Project Members, 2013: Onset of deglacial warming in West Antarctica driven by local orbital forcing. *Nature*, **500**, 440–444, https://doi.org/10.1038/nature12376.

Watanabe, O., S. J. J. Jouzel, F. Parrenin, H. Shoji, and N. Yoshida, 2003: Homogeneous climate variability across East Antarctica over the past three glacial cycles. *Nature*, **422 (693)**, 509–512, https://doi.org/10.1038/nature01525.

Wong, T. E., J. Nusbaumer, and D. C. Noone, 2017: Evaluation of modeled land-atmosphere exchanges with a comprehensive water isotope fractionation scheme in version 4 of the Community Land Model. *J. Adv. Model. Earth Sy.*, **9 (2)**, 978–1001, https://doi.org/10.1002/2016MS000842.

Accepted for publication in *Journal of Climate*. DOI 10.1175/JCLI-D-22-0647.1.